







Galaxy Structure in the Ultraviolet: The Dependence of Morphological Parameters on Rest-frame Wavelength

Violet A. Mager¹, Christopher J. Conselice² , Mark Seibert³ , Courtney Gusbar⁴, Anthony P. Katona⁵, Joseph M. Villari⁵, Barry F. Madore³ , and Rogier A. Windhorst⁶ 

¹ Pennsylvania State University Wilkes-Barre, Old Route 115, Lehman, PA 18627, USA; vam5238@psu.edu

² University of Nottingham, School of Physics and Astronomy, University Park, Nottingham NG7 2RD, UK; christopher.conselice@nottingham.ac.uk

³ Carnegie Observatories, 813 Santa Barbara Street, Pasadena, CA 91101, USA; mseibert@obs.carnegiescience.edu, barry@obs.carnegiescience.edu

⁴ Ohio University, Department of Physics and Astronomy, Athens, OH 45701, USA

⁵ Susquehanna University, Department of Physics, 514 University Avenue, Selingsgrove, PA 17870, USA

⁶ Arizona State University, School of Earth & Space Exploration, Tempe, AZ 85287-1404, USA; Rogier.Windhorst@asu.edu

Received 2017 February 1; revised 2018 June 21; accepted 2018 July 8; published 2018 September 5

Abstract

Evolutionary studies that compare galaxy structure as a function of redshift are complicated by the fact that any particular galaxy’s appearance depends in part on the rest-frame wavelength of the observation. This leads to the necessity for a “morphological k-correction” between different passbands, especially when comparing the rest-frame optical or infrared (IR) to the ultraviolet (UV). This is of particular concern for high-redshift studies that are conducted in the rest-frame UV. We investigate the effects of this “bandpass shifting” out of the UV by quantifying nearby galaxy structure via concentration, asymmetry, and clumpiness (CAS) parameters. For this study we combine panchromatic data from the UV through the near-IR with *Galaxy Evolution Explorer* (GALEX) data of 2073 nearby galaxies in the “near-UV” (NUV; ~ 230 nm) and 1127 in the “far-UV” (FUV; ~ 150 nm), providing the largest study of this kind in the mid- to far-UV. We find a relationship between the CAS parameters and observed rest-frame wavelength that make galaxies appear more late-type at shorter wavelengths, particularly in the UV. The effect is strongest for E/S0 galaxies in the far-UV, which have concentrations and asymmetries that more closely resemble those of spiral and peculiar/merging galaxies in the optical. This may be explained by extended disks containing recent star formation. Here, we also release the CAS values of the galaxies imaged in GALEX NUV and FUV for use in comparisons with deep *Hubble Space Telescope* imaging and the *James Webb Space Telescope* in the future.

Key words: galaxies: evolution – galaxies: structure

Supporting material: machine-readable tables

1. Introduction

The majority of high-redshift ($z > 2$) galaxies appear similar to a relatively rare subset of low-redshift irregular and peculiar galaxies, whose morphologies appear to be pathological due to mergers or interactions (e.g., Driver et al. 1995; Conselice et al. 2005; Kriek et al. 2009; Delgado-Serrano et al. 2010; Mortlock et al. 2013). This observed increase in the percentage of apparently merging/interacting galaxies with redshift supports models of hierarchical galaxy formation (e.g., Nagashima et al. 2002).

Comparison studies of galaxies at different redshifts are complicated, however, by the fact that galaxies can appear substantially different at shorter wavelengths than at longer ones (e.g., Bohlin et al. 1991; Kuchinski et al. 2000; Windhorst et al. 2002). This is especially true for galaxies that appear as earlier types at the longer wavelengths. This leads to a “morphological k-correction” for a given galaxy between different rest-frame wavelengths. This is particularly important in studies of high-redshift galaxies, as bandpass shifting will cause light originally emitted in the UV to be shifted as far as the IR by the time it reaches Earth. This raises questions about how much of the irregular/peculiar morphologies seen in high-redshift studies are simply due to bandpass shifting, and not due to real differences in galaxy type. Kuchinski et al. (2001) showed that this effect alone is enough to misclassify galaxies as peculiar when simulated at higher redshifts.

A quantitative measurement of the morphological k-correction is therefore an essential first step in the study of galaxy evolution.

This correction is expected to be particularly significant when comparing the rest-frame UV to the optical or IR, as galaxy stellar energy distributions can change drastically shortward of the Balmer Break ($\lambda_c \lesssim 360$ nm), and UV-bright star-forming regions dominate galaxy morphology that appears to be smoother at redder wavelengths. To determine the extent of this effect, it is critical to conduct a large representative benchmark study at $z \simeq 0$. This is complicated by the difficulty of observing in the UV through the atmosphere: it is necessary to use space-based telescopes with UV sensitive detectors, such as *Hubble Space Telescope* (HST) and *Galaxy Evolution Explorer* (GALEX). Throughout its operation, GALEX has amassed the largest image database in the far-UV to date (Bianchi & GALEX Science Team 1999; Martin & GALEX Science Team 2005, 2009). This makes GALEX ideal for these types of studies, where large number statistics are needed to determine overall generalized trends in galaxy structure.

One of the most efficient ways to quantify the morphological k-correction is through measurements of the concentration, asymmetry, and clumpiness (CAS) parameters of galaxies as a function of their rest-frame wavelength. The concentration of light as it is radially distributed within a galaxy (C) correlates with the stellar and kinematic masses of

galaxies. The degree to which a galaxy deviates from perfect symmetry (A) can indicate ongoing galaxy mergers or interactions. The proportion of high-frequency structure to the smooth light distribution of a galaxy (S) correlates with current star formation (Conselice 2003). Conselice (2006) argues that these parameters are the more fundamental properties that describe a galaxy’s physical state, and thus are a good, objective way of classifying galaxies. Nearby galaxy studies have shown that a combination of these parameters provides a relatively robust automated galaxy classification system, which can be used to determine the nature of the population distributions for large samples of galaxies (e.g., Bershadsky et al. 2000; Conselice 2003, 2006). In Taylor-Mager et al. (2007), we found that earlier-type galaxies are on average increasingly more concentrated, more symmetric, and less clumpy than later-type galaxies. Merging galaxies occupy separate locations within the CAS parameter space, which leads to a clear and efficient method of automatically identifying merging galaxies.

There have been a few studies that quantify the morphological k -correction of nearby ($z \sim 0$) galaxies (e.g., Bohlin et al. 1991; Windhorst et al. 2002; Vika et al. 2013), one of the largest of which is our earlier project (Taylor-Mager et al. 2007) that utilized multiwavelength (0.15–0.85 μm) CAS measurements of 199 galaxies. Only a subset of this sample had UV data at the time, with *GALEX* observations for just 14 of them. Due to signal-to-noise ratio (S/N) and resolution constraints, only seven galaxies were used to calculate the final k -correction in the NUV ($\lambda_c = 2275 \text{ \AA}$) and five in the FUV ($\lambda_c = 1550 \text{ \AA}$). Complementary *HST* WFPC2 data allowed for measurements at longer UV wavelengths, with eight galaxies in the F255W ($\lambda_c = 2550 \text{ \AA}$) filter and 86 in F300W ($\lambda_c = 2930 \text{ \AA}$). Galaxy number statistics were small in the UV for all galaxy types, but particularly for early-type (E-S0) galaxies, which were not the focus of that study and which are especially faint in the UV due to their intrinsically red colors. As such, we were unable to provide a reliable quantified measure of the morphological k -correction in the UV for E-S0 galaxies in that paper. We noted an intriguing trend of E-S0 galaxies apparently becoming dramatically less concentrated in the UV, but included the caveat that this needed to be verified with a larger sample of early-type galaxies.

This has motivated our present study, which uses images in the *GALEX* archive to drastically improve our number statistics (by up to almost a factor of 300) in the far- to mid-UV, providing the largest analysis of the wavelength dependence of nearby galaxy CAS structure in this wavelength range to date.

2. Data Analysis

Conselice (2003) and Conselice et al. (2000) showed that poor spatial resolution and low S/N affect the reliability of CAS measurements. As such, we applied the selection criteria of $S/N \geq 75$ and linear resolution $\leq 1.25 \text{ kpc}$ to our sample. These limits are more relaxed than the upper limits determined in Conselice et al. (2000; $S/N \geq 100$ and resolution $\leq 1 \text{ kpc}$), but were chosen to be consistent with the combined ground-based and *HST* sample (Taylor-Mager et al. 2007), for which we determined that these relaxed limits did not have a significant impact on the CAS measurements and allowed for improved number statistics. Our resolution-limited sample

contains 2967 galaxies in the *GALEX* GR6 data release⁷ that have images in at least the NUV filter. Applying the S/N cut (see below for details on how it was calculated) reduced the sample to 2073 galaxies in NUV and 1127 galaxies in FUV. A histogram of S/N values is shown in Figure 1. Figure 2 displays example images of galaxies with three different S/N in NUV. The top left galaxy meets our relaxed requirement of $S/N \geq 75$, but falls short of the more strict requirement of $S/N \geq 100$. The top right galaxy has an S/N just over 100, and the bottom galaxy has a particularly high S/N of over 1000.

We processed the images using the pipeline designed by the *GALEX* team for creating extended source catalogs (Seibert et al. 2012), which are published as the *GALEX* All-Sky Survey Source Catalog (GASC) and Medium Imaging Survey Source Catalog (GMSC). Parameters such as the position of the galaxy center, size, ellipticity, and inclination were found using the pipeline’s automated software and then were verified by eye, with corrections made as necessary if the target galaxy was not properly parameterized by the automated algorithm. Non-target sources bright and close enough to the target galaxy to significantly affect photometry were manually identified and marked for inclusion in a mask file. In this initial step, we removed only these sources from our images by interpolating over them. From the panchromatic object counts of Windhorst et al. (2011, their Figures 11 and 12), we expect an integrated 10 galaxies deg^{-2} to $AB < 15 \text{ mag}$ in the V band. From Windhorst et al. (2008), the median half-light radius $r_{hl} < 0.5 \text{ arcmin}$ at $V < 15 \text{ mag}$, so the area in the sky covered by galaxies with $V < 15 \text{ mag}$ is $< 7.8 \text{ arcmin}^2$. The star counts of Windhorst et al. (2011, their Figure 11) have an integrated 200–500 stars deg^{-2} (valid for a range of b_{II}) to $V < 15 \text{ mag}$, or < 0.056 – 0.14 arcmin^{-2} . The areal ratio of stars/galaxies in the sky to $AB < 15 \text{ mag}$ is therefore $< 0.7\%$ – 1.8% , i.e., generally less than 2% of nearby galaxies will have been affected by a Galactic star. Also, only a few percent of nearby galaxies have close companions (e.g., Mantha et al. 2018). Hence, no more than a few percent of all target galaxies will have been affected by stars or neighboring galaxies, which were masked out in the standard *GALEX* processing stage.

All other non-target sources were excluded while measuring CAS parameters as described in the next paragraph. The S/N of each galaxy was calculated using the following formula, the image exposure time (exptime), the total object counts per second (int) above the local sky-value, and the background counts per second (bg), as measured by the *GALEX* pipeline process (Seibert et al. 2012):

$$S/N = \frac{\text{int} \times \text{exptime}}{\sqrt{\text{exptime} \times (\text{int} + \text{bg})}}. \quad (1)$$

In our previous study (Taylor-Mager et al. 2007), we removed all non-target sources from our images before feeding them into the automated IRAF⁸ task CAS, developed by C. Conselice (Conselice et al. 2000; Conselice 2003). In this earlier version of the CAS software, a region of empty sky was chosen for background calculations. For this study, we use an

⁷ galex.stsci.edu/GR6

⁸ IRAF is distributed by the National Optical Astronomy Observatories, which are operated by the Association of Universities for Research in Astronomy, Inc., under cooperative agreement with the National Science Foundation.

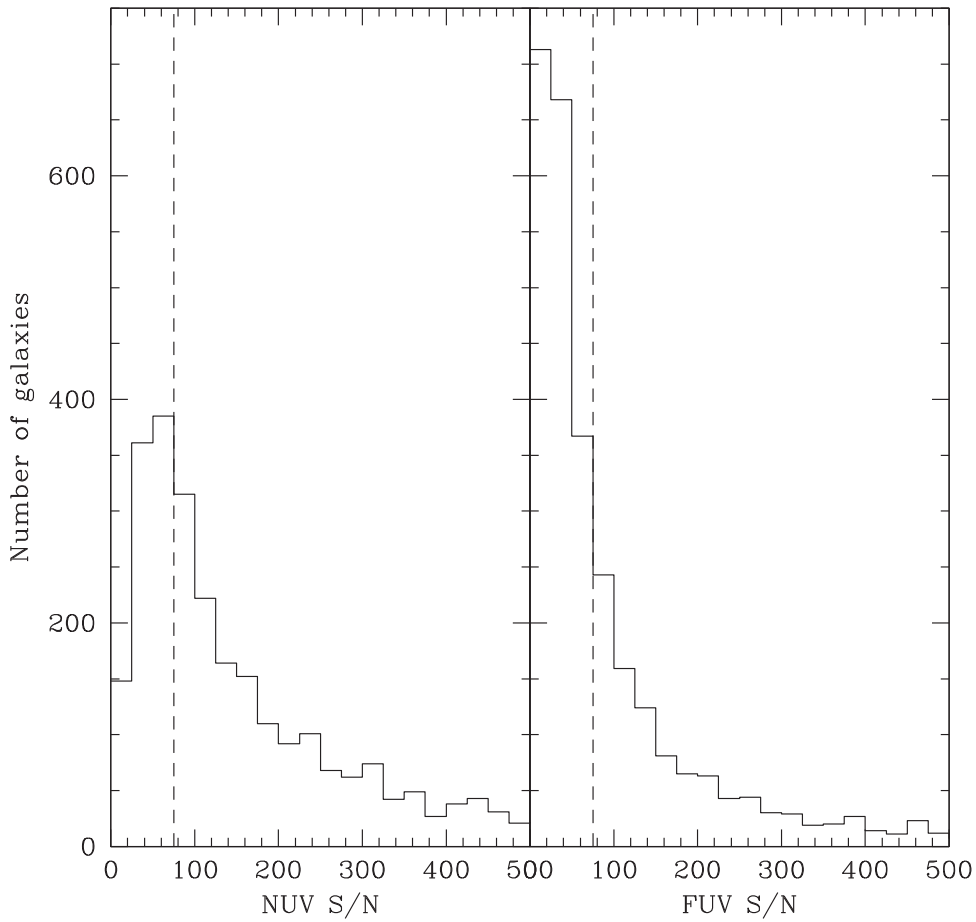


Figure 1. Histogram of signal-to-noise ratios (S/Ns) of *GALEX* NUV (left panel) and FUV (right panel) galaxies in our initial sample. Only galaxies with $S/N \geq 75$ were used in our analysis (dotted line). Not shown here are 120 galaxies in FUV and 462 in NUV with $S/N > 500$.

improved version of the CAS software, which uses a more accurate method of measuring the sky. Source segmentation maps are produced by SExtractor (Bertin & Arnouts 1996) and used by the CAS code to remove contaminating objects, replacing them with a local sky background including its proper noise characteristics. We used this CAS code to measure the CAS parameters as defined by Conselice et al. (2000) and Conselice (2003), as described below.

The concentration index, C , is computed by determining the total sky-subtracted light contained within $1.5 \times$ the galaxy’s Petrosian radius (r_{Pet} ; Petrosian 1976) and finding the logarithmic ratio of the radius within which 80% of this light is contained (r_{80}) to the radius within which 20% of this light is contained (r_{20} ; Conselice et al. 2000). The concentration index is thus given by the formula

$$C = 5 \times \log(r_{80}/r_{20}). \quad (2)$$

Galaxies that are highly concentrated in their centers will have high values of C , and galaxies that have less centrally concentrated light distributions will have lower values of C .

The asymmetry index, A , is computed by rotating the galaxy by 180° from its center and subtracting the light within $1.5 \times r_{\text{Pet}}$ in the rotated image (I_{180}) from that in the original image (I_o). The ratio of the residual subtracted flux to the

original galaxy flux yields A :

$$A = \min\left(\frac{\sum |I_o - I_{180}|}{\sum |I_o|}\right) - \min\left(\frac{\sum |B_o - B_{180}|}{\sum |I_o|}\right). \quad (3)$$

Noise corrections are applied by subtracting the asymmetry of the sky (B), and iterative centering corrections are applied to minimize A , since gross centering errors would artificially increase the derived A -values. The center used to minimize A was not used for the concentration index, which instead utilized the centroid of light. Conselice (2003) found a difference of at most a few pixels between these centers, or roughly 2% the size of the galaxy, and the center choice had no effect on the determination of C , even to within 5%–10% of the size of the galaxy. Asymmetries range from $A = 0$ to 2, with $A = 0$ corresponding to a truly symmetric galaxy and $A = 2$ corresponding to a very asymmetric galaxy.

The clumpiness index, S , is defined as the ratio of the amount of light in high spatial frequency structures within $1.5 \times r_{\text{Pet}}$ to the total amount of light in the galaxy within that radius (Conselice 2003). This is done by subtracting a boxcar-smoothed image from the original image to produce an image that contains *only* its high-frequency structure. The central pixels within $1/20$ th of the total radius ($1.5 \times r_{\text{Pet}}$) are set to zero to exclude them from the parameter measurements. S is given by the following equation, where $I_{x,y}$ is the intensity of

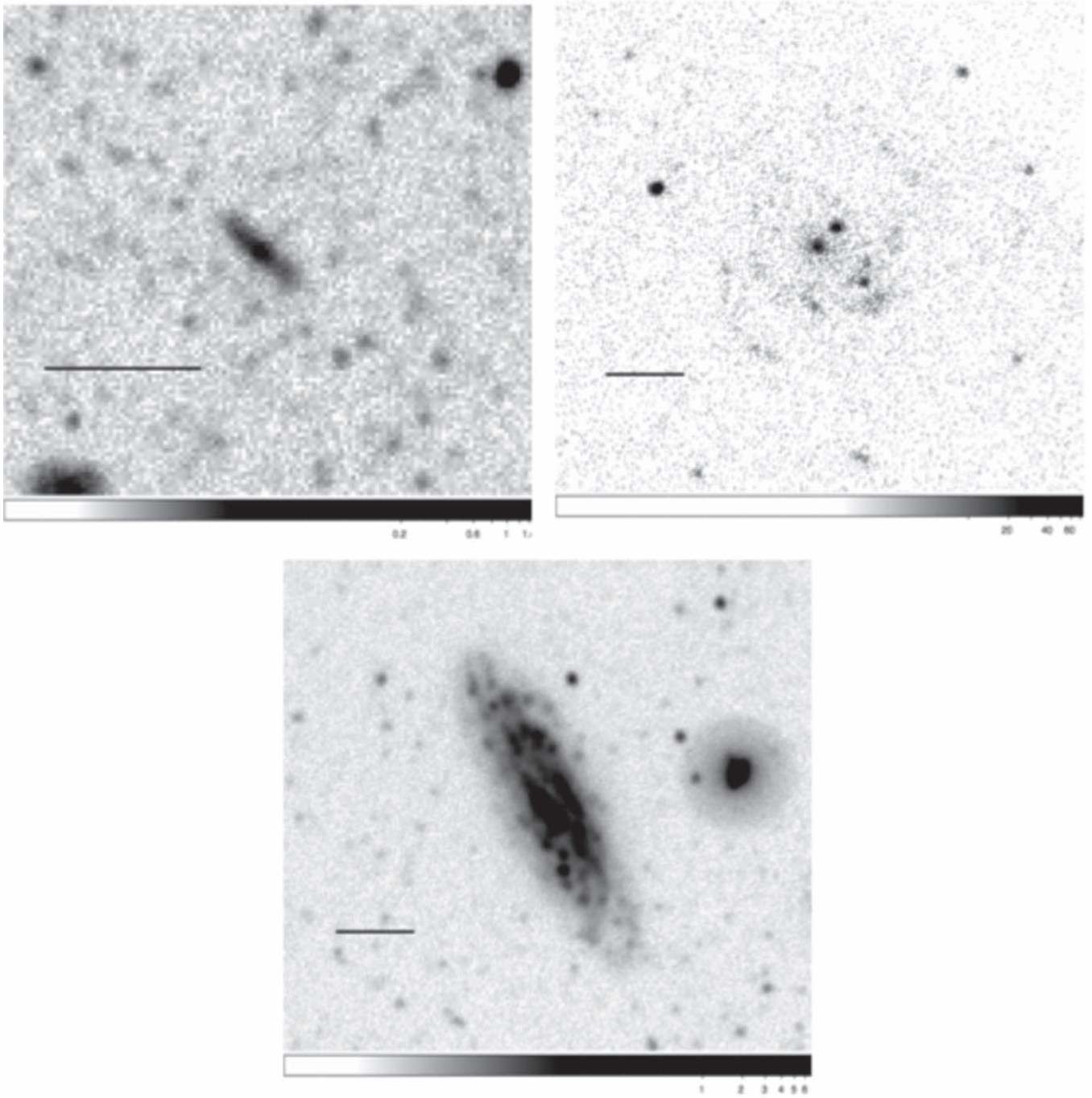


Figure 2. Examples of some galaxies of different quality in signal-to-noise ratio (S/N) in the *GALEX* NUV filter. The horizontal line marks a length of ~ 1 arcmin (40 pixels). Top left: 2MASX J11102621+5824080, with an S/N of 88. Top right: ESO 119-048, with an S/N of 123. Bottom: ESO 116-012, with an S/N of 1330.

light in a given pixel, $I_{x,y}^s$ is the intensity of that pixel in the image smoothed by $0.3 \times r_{\text{Pet}}$, and $B_{x,y}^s$ is an intensity value of a pixel from a smoothed background region:

$$S = 10 \times \left(\frac{\sum_{x,y=1,1}^{N,N} (I_{x,y} - I_{x,y}^s)}{\sum_{x,y=1,1}^{N,N} I_{x,y}} - \frac{\sum_{x,y=1,1}^{N,N} B_{x,y}^s}{\sum_{x,y=1,1}^{N,N} I_{x,y}} \right). \quad (4)$$

A clumpiness of $S = 0$ corresponds to a galaxy that has no high-frequency structure and is therefore completely smooth. Galaxies with more high-frequency structure are more patchy in appearance and so will have a higher value of S .

3. Results

3.1. GALEX CAS Analysis

Table 1 lists the galaxies in our sample and their CAS parameters as measured in the NUV and FUV, for which $S/N \geq 75$. Table 2 lists CAS parameters for galaxies that had $S/N < 75$ in the NUV and/or FUV. The first 10 galaxies are listed here, with the full tables available in machine-readable format. Types were obtained from the homogenized galaxy morphology classification listed in the NASA/IPAC Extragalactic Database (NED), and each galaxy was placed into a numerical type category defined as follows: 1 = E-S0

Table 1
High-S/N Measured CAS Parameters

Galaxy ...	R.A. (deg) S/N _{NUV}	Decl. (deg) S/N _{FUV}	Type ...	C _{NUV} $\sigma_{C_{NUV}}$	A _{NUV} $\sigma_{A_{NUV}}$	S _{NUV} $\sigma_{S_{NUV}}$	C _{FUV} $\sigma_{C_{FUV}}$	A _{FUV} $\sigma_{A_{FUV}}$	S _{FUV} $\sigma_{S_{FUV}}$
2MASX J11102621+5824080	167.60939026	58.40214920	2	3.066	0.189	0.200	9.999	9.999	9.999
...	88.3	30.4	...	0.163	0.047	0.018	9.999	9.999	9.999
ESO 013-016	23.19899900	-79.47364800	3	2.313	0.554	0.260	9.999	9.999	9.999
...	146.1	67.9	...	0.053	0.026	0.006	9.999	9.999	9.999
ESO 026-001	306.24542200	-81.57592000	2	1.891	0.465	0.320	9.999	9.999	9.999
...	84.5	36.5	...	0.046	0.110	0.013	9.999	9.999	9.999
ESO 048-017	332.23184200	-73.38194300	3	2.543	0.611	0.300	9.999	9.999	9.999
...	141.8	40.2	...	0.064	0.092	0.009	9.999	9.999	9.999
ESO 079-003	8.00970000	-64.25241466	2	3.662	0.589	0.370	9.999	9.999	9.999
...	87.2	32.9	...	0.100	0.071	0.009	9.999	9.999	9.999
ESO 079-005	10.18214028	-63.44262759	4	2.937	0.954	0.260	9.999	9.999	9.999
...	94.8	45.3	...	0.055	0.060	0.006	9.999	9.999	9.999
ESO 079-007	12.51660000	-66.55376752	4	2.514	0.482	0.280	9.999	9.999	9.999
...	174.8	43.7	...	0.067	0.019	0.005	9.999	9.999	9.999
ESO 085-014	73.66965500	-62.80207100	3	3.679	0.962	0.290	4.213	0.787	0.170
...	445.6	145.3	...	0.079	0.041	0.004	0.106	0.074	0.005
ESO 085-030	75.37484742	-63.29272843	4	2.625	0.316	0.160	9.999	9.999	9.999
...	155.7	74.2	...	0.106	0.016	0.003	9.999	9.999	9.999
ESO 085-038	76.07969999	-63.58132935	2	2.273	0.500	0.090	9.999	9.999	9.999
...	82.9	34.8	...	0.059	0.100	0.004	9.999	9.999	9.999

Note. CAS parameters and their uncertainties in the NUV and FUV for galaxies in our sample that were used for this study, with signal-to-noise ratio $S/N_{\text{NUV}} \geq 75$. CAS values and their errors in the FUV are set to 9.999 for a null value (when $S/N < 75$). Galaxy type is listed as defined in Section 3. Coordinates are given in J2000.

(This table is available in its entirety in machine-readable form.)

Table 2
Low-S/N Measured CAS Parameters

Galaxy ...	R.A. (deg) S/N _{NUV}	Decl. (deg) S/N _{FUV}	Type ...	C _{NUV} $\sigma_{C_{NUV}}$	A _{NUV} $\sigma_{A_{NUV}}$	S _{NUV} $\sigma_{S_{NUV}}$	C _{FUV} $\sigma_{C_{FUV}}$	A _{FUV} $\sigma_{A_{FUV}}$	S _{FUV} $\sigma_{S_{FUV}}$
2MASX J11102621+5824080	167.60939026	58.40214920	2	3.066	0.189	0.200	2.853	0.247	0.130
...	88.3	30.4	...	0.163	0.047	0.018	0.167	0.059	0.038
2MASX J11554657+2956291	178.94429016	29.94148064	2	2.766	0.581	0.170	3.134	-0.15	0.000
...	34.6	14.3	...	0.095	0.105	0.010	0.151	0.210	0.000
2MASX J16052284-0002177	241.34519958	-0.03841000	5	2.485	-0.09	-0.48	2.045	0.733	-0.07
...	24.5	6.5	...	0.109	0.190	0.020	0.127	0.270	0.009
ESO 002-006	3.71070004	-86.99308012	1	3.195	1.000	0.000	1.950	1.071	0.000
...	12.5	80.0	...	0.173	0.174	0.000	0.144	0.302	0.000
ESO 005-009	112.47719761	-84.03832244	3	2.164	0.781	0.260	9.999	9.999	9.999
...	42.8	0.0	...	0.092	0.088	0.009	9.999	9.999	9.999
ESO 013-007	14.99880028	-79.95686341	1	2.491	-0.38	0.000	0.000	0.220	0.000
...	10.5	3.6	...	0.243	0.197	0.000	0.369	0.381	0.000
ESO 013-016	23.19899900	-79.47364800	3	2.313	0.554	0.260	2.435	0.947	0.350
...	146.1	67.9	...	0.053	0.026	0.006	0.051	0.048	0.013
ESO 026-001	306.24542200	-81.57592000	2	1.891	0.465	0.320	1.951	1.140	0.520
...	84.5	36.5	...	0.046	0.110	0.013	0.043	0.134	0.022
ESO 047-034	322.93289186	-76.48059845	1	3.027	0.251	0.000	0.000	-1.96	0.000
...	12.9	4.1	...	0.249	0.257	0.000	0.369	0.206	0.000
ESO 048-017	332.23184200	-73.38194300	3	2.543	0.611	0.300	2.345	0.643	0.340
...	141.8	40.2	...	0.064	0.092	0.009	0.061	0.105	0.016

Note. CAS parameters and their uncertainties in the NUV and FUV for galaxies in our sample that have signal-to-noise ratio $S/N < 75$ in one or both filters, which were rejected in our analysis. We advise against using data with $S/N < 30$ in structure and morphology studies. CAS values and their errors in the FUV are set to 9.999 for a null value (when no data exist). Galaxy type is listed as defined in Section 3. Coordinates are given in J2000.

(This table is available in its entirety in machine-readable form.)

(elliptical and lenticular), 2 = Sa-Sc (“early-type” spirals), 3 = Sd-Im (“late-type” spirals and irregulars), and 4 = peculiar or merging. All galaxies that had a peculiar (pec) designation in their classification were placed in the fourth type bin, regardless

of any other designation they may have also had. Galaxies that could not be placed into any of these categories were given no type (such as those without any classification listed in NED or nonspecific classifications such as $S?$).

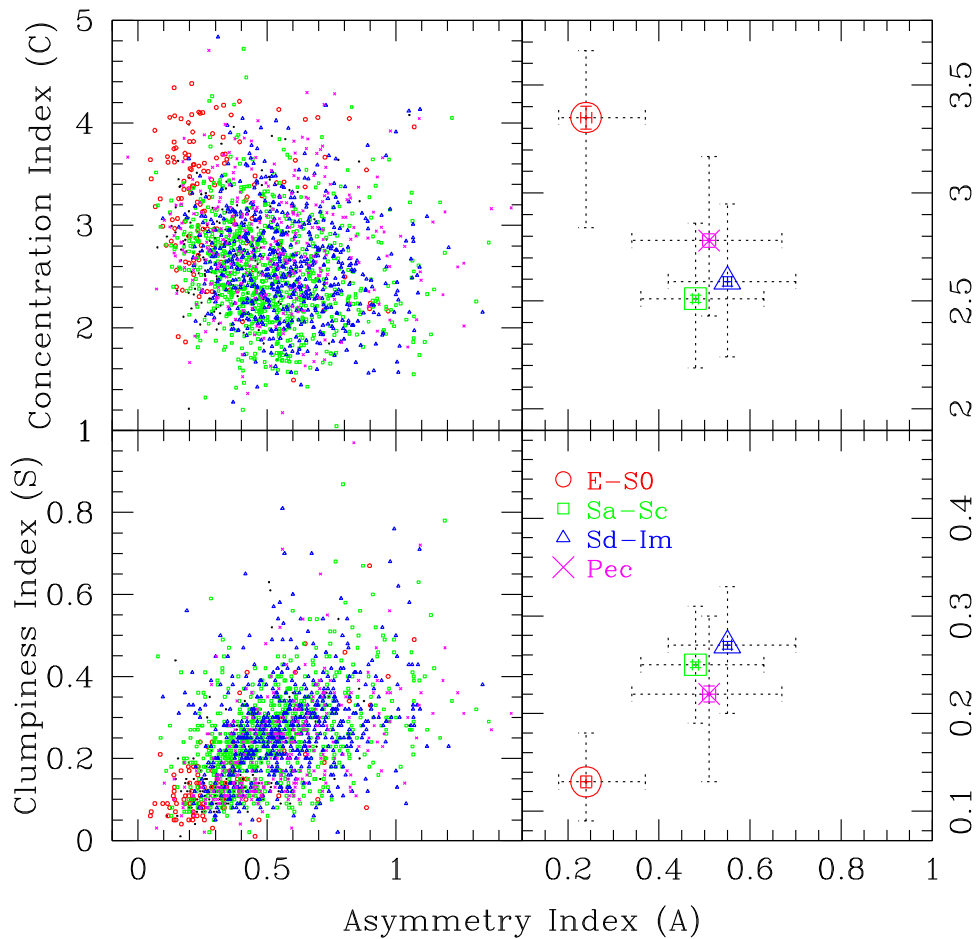


Figure 3. CAS parameter space for individual galaxies in the NUV (left) and for the median values per galaxy type bin (right). Dotted error bars indicate the 25%–75% quartile range. Solid error bars indicate the error on the median and are on the order of the size of the data points, or smaller. Galaxies without an assigned type are plotted with tiny solid black circles. A general trend exists of galaxies with increasingly higher asymmetry becoming less concentrated and more clumpy. Although there is a fair amount of overlap in CAS parameters by galaxy type, the median values reveal that on average galaxies with progressively earlier Hubble type have higher concentrations, lower asymmetries, and lower clumpiness.

We plot each galaxy in “CAS space” (concentration and clumpiness versus asymmetry) in the left panels of Figure 3 for the NUV and Figure 4 for the FUV, with symbols coded by galaxy type. Median values with their errors (solid error bars) and 25%–75% quartile ranges (dotted error bars) for each type bin are plotted in the right panels. Median values were calculated from 134 E/S0, 852 Sa-Sc, 600 Sd-Im, and 312 Pec galaxies in the NUV and 56 E/S0, 485 Sa-Sc, 364 Sd-Im, and 157 Pec galaxies in the FUV, when using the criteria that $S/N \geq 75$.

We tested how the median values would be affected by a stricter limit of $S/N \geq 100$ and found no difference within the errors for all but two of the data points (NUV C for Sa-Sc and FUV A for Sd-Im), which differed (S/N cut at 100 minus S/N cut at 75) by -0.03 ± 0.02 , a 1.5σ difference. The number of E/S0 galaxies was lowered from 134 to 106 in the NUV and 56 to 37 in the FUV. Since there was little to no effect on our results by using the stricter S/N constraint, to remain consistent with the *HST*/Vatican Advanced Technology Telescope (VATT) data and to preserve higher number statistics for the underrepresented E/S0 galaxies, we continue with the $S/N \geq 75$ constraint.

As seen in Figures 3 and 4, while there is a significant amount of overlap between galaxy types, there is an overall average trend of galaxies in both passbands tending to appear

less concentrated, more clumpy, and more asymmetric when progressing from early-type (E/S0) through late-type (Sd-Im) galaxies on the Hubble sequence. This same effect is also apparent in the near-UV through near-IR (NIR; Taylor-Mager et al. 2007) and coincides with the expectations, since later-type galaxies are known to have lower bulge-to-disk ratios (and thus a higher percentage of light in the extended outer regions) and more recent star formation (which contributes to clumpy regions and an overall asymmetry).

The peculiar galaxy category contains many different types of galaxies, from full-on major mergers to otherwise normal elliptical or spiral galaxies that contain some level of unusual structure. It is therefore not surprising that their median values in Figures 3 and 4 fall near the average of all galaxy types, although they do tend to be slightly more concentrated than the average normal spiral. In Taylor-Mager et al. (2007), we found a progression through merger stages, where galaxies initially become significantly less concentrated and more asymmetric and clumpy, then settle back closer to the locus of normal galaxies as post-mergers. The concentration indices of these post-mergers, however, are notably higher than the average normal spiral galaxy, as gas was funneled into the center by the merger process. This suggests that our peculiar category is dominated by post-mergers, with the presence of visible tidal or “disturbed” features leading to the “peculiar” classification.

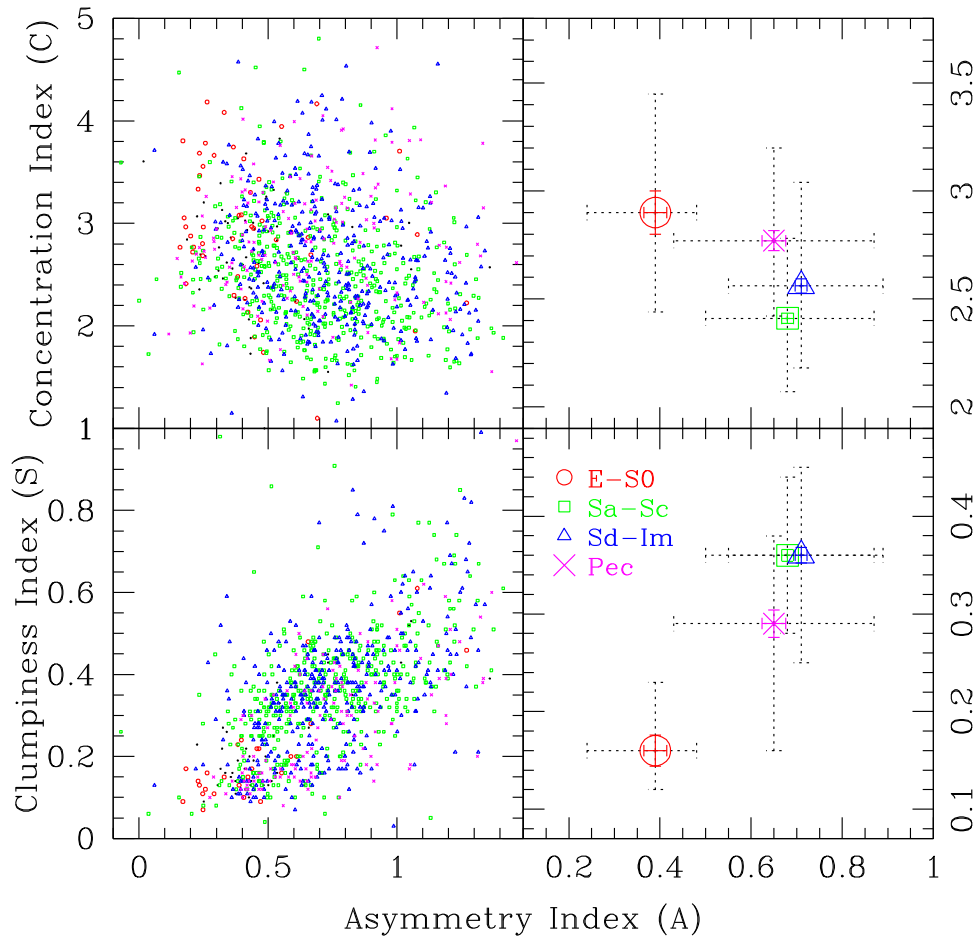


Figure 4. Same as in Figure 3, but with CAS parameters plotted for galaxies in the FUV. Similar general trends are apparent in the FUV as in the NUV (Figure 3).

Comparing the median values in Figures 3 and 4 reveals that E/S0 galaxies are on average significantly less concentrated and more asymmetric in the FUV than in the NUV, and later galaxy types are significantly more asymmetric and clumpy in the FUV than in the NUV.

3.2. CAS Wavelength Dependence

Figure 5 shows the relationship of the median CAS parameters for each type bin with observed rest-frame wavelength. Here, we supplement the FUV and NUV results from this study with data used in our previous study (Taylor-Mager et al. 2007), which includes *HST* WFPC2 mid- to near-UV (F255W, $\lambda_c = 255$ nm and F300W, $\lambda_c = 293$ nm) and NIR data (F814W, $\lambda_c = 823$ nm), as well as ground-based UBV R ($\lambda_c = 360, 436, 540,$ and 634 nm, respectively) data from the VATT. Solid error bars indicate the error on the median, while dashed error bars give the 25%–75% quartile ranges, which indicate the spread of the data. The number statistics in the FUV and NUV are vastly improved in this study, which has resulted in much smaller error bars for each of the spiral, irregular, and peculiar galaxy type categories.

For Figure 5 we reprocessed the Taylor-Mager et al. (2007) data through the newest version of the CAS code, as it treats background removal differently (utilizing the entire image with objects masked out via SExtractor catalogs versus a small user-defined box of empty sky). This had a minor impact on a small number of data points as compared to our 2007 results from the previous version of the code, but the overall trends with

wavelength remain the same. This demonstrates that the difference in background subtraction methods does not have a significant impact on our conclusions. We rejected any median data points derived from fewer than five *HST* galaxies, as these low number statistics would produce unreliable results.

Most panels in Figure 5 show a consistent general trend in CAS values as a function of rest-frame wavelength. A major exception is the clumpiness (S) parameter for all galaxy types except E/S0, where S increases significantly with decreasing wavelength, then drops dramatically between the *HST*/VATT UV and the shorter *GALEX* NUV wavelength (the second data point from the left in each panel). The clumpiness parameter is particularly sensitive to the image resolution, as the high-frequency structure measured by the S value is smoothed out in low-resolution images. The *GALEX* images (left two data points in each panel) have a stellar FWHM of 5 arcsec, while the VATT and the convolved *HST* images from Taylor-Mager et al. (2007) have an average stellar FWHM of 1.75 arcsec.⁹

To test the effect of image resolution, we convolved the *HST* F300W images to the *GALEX* resolution and measured the resulting median CAS values. We found no change within the uncertainties for any of the E/S0 CAS values and no change in C and A for the peculiar galaxies and C for Sa-Sc. There was a minor (1.6σ) decrease in A for Sa-Sc and Sd-Im at the poorer

⁹ For Taylor-Mager et al. (2007), all images were convolved with a differential point-spread function (PSF), such that the total PSF in all images had an FWHM ~ 1.75 . In the current study, we do not convolve all data to the coarse *GALEX* FWHM in order to better see the optical trends.

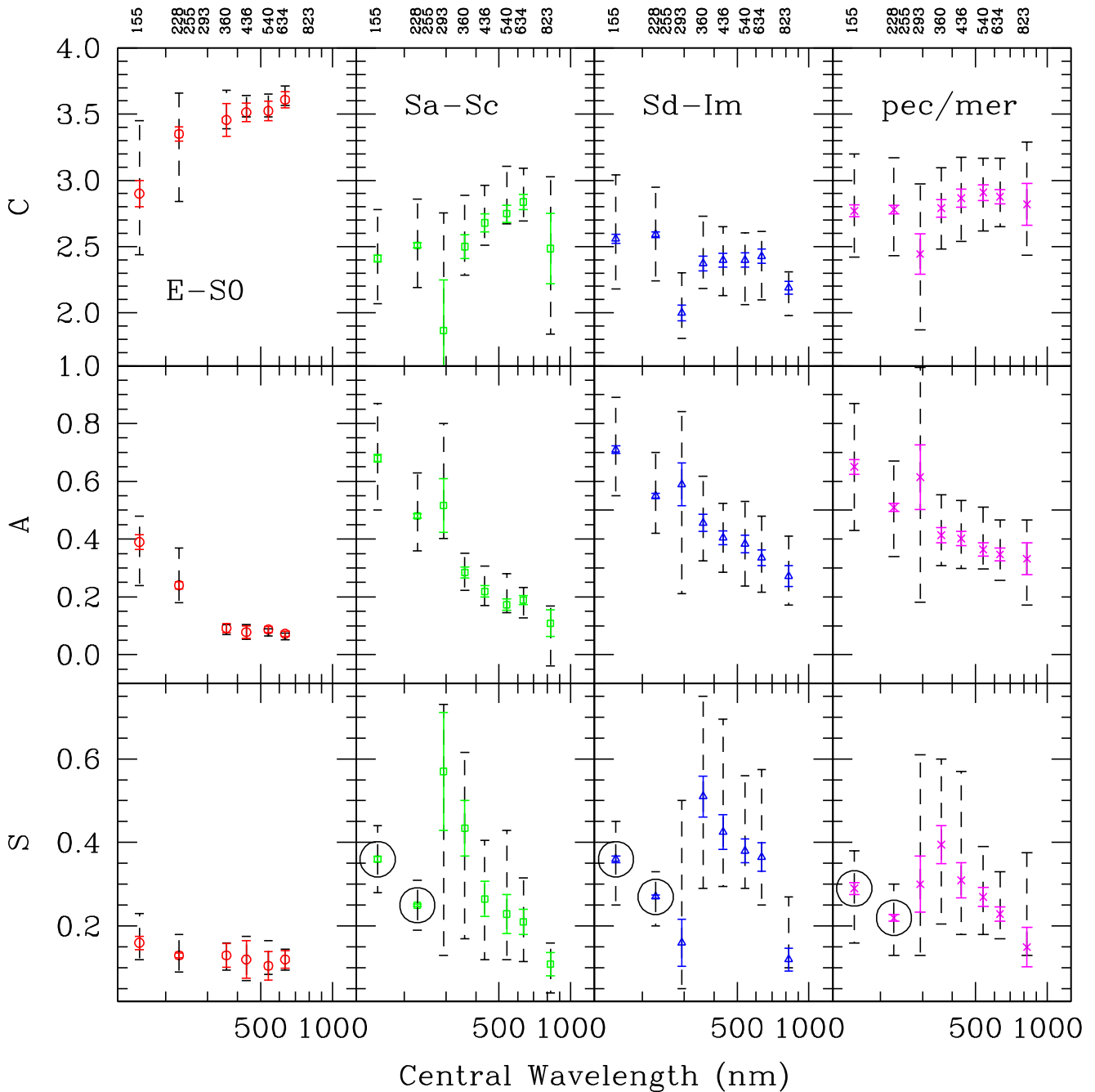


Figure 5. Median CAS values in each type bin as a function of wavelength. Solid error bars indicate the error on the median, and dashed error bars indicate the 25%–75% quartile range of the data. The *GALEX* data (two left-most data points in each panel) are supplemented with *HST* and ground-based data. Circled data points: low *GALEX* S values are due to its poor (5 arcsec stellar FWHM) resolution. Disregarding this effect results in higher S values more in line with the trend displayed at longer wavelengths. In general, galaxies are more asymmetric and more clumpy at shorter rest-frame wavelengths, especially in the UV. This causes them to appear overall later type than they would at longer wavelengths. Sa-Sc galaxies appear less concentrated at shorter wavelengths, while Sd-Im and pec/mer galaxies do not exhibit a strong concentration versus wavelength relationship. The effect in the UV is particularly pronounced for elliptical/lenticular galaxies, which have little difference in their CAS parameters in the near-UV through the NIR, but appear significantly less concentrated, more asymmetric, and slightly more clumpy in the far-UV.

resolution and a 2.1σ increase in C for Sd-Im. As expected, the S values were generally impacted the most, with a decrease of 3.4σ , 1.2σ , and 2.3σ for Sa-Sc, Sd-Im, and pec/mer, respectively. We therefore conclude that there is an artificial systematic baseline difference due to differences in resolution for some of the panels in Figure 5. This explains the discrepancy in wavelength dependence between the *GALEX* NUV and *HST* F300W or VATT U-band data, as removing the effect would result in *GALEX* measurements that are significantly higher in S for all but the E/S0 galaxies (Sa-Sc:

0.48 ± 0.14 , Sd-Im: 0.06 ± 0.05 , and pec/mer: 0.18 ± 0.08), slightly higher in A for Sa-Sc (0.21 ± 0.13) and Sd-Im (0.14 ± 0.09), and slightly lower in C for Sd-Im (-0.17 ± 0.08). As these corrections were measured in F300W, we do not apply them to the *GALEX* data in Figure 5, but consider their effects in our discussion of the results below.

Early- to mid-type spirals (Sa-Sc) are generally less concentrated and more asymmetric and clumpy at increasingly shorter observed wavelengths. Although the two shortest-wavelength data points (*GALEX* NUV/FUV) have much lower

Table 3
CAS UV Wavelength Dependence

Type Bin	δ_C	σ_C	δ_A	σ_A	δ_S	σ_S
E/S0	0.45	0.11	-0.15	0.03	-0.03	0.02
Sa-Sc	0.10	0.03	-0.20	0.01	-0.11	0.01
Sd-Im	0.03	0.04	-0.16	0.02	-0.09	0.01
Pec	0.01	0.06	-0.14	0.03	-0.07	0.02

Note. The dependence of the CAS parameters on UV wavelength. δ is defined as the median NUV CAS parameter for a given galaxy type bin minus the median FUV CAS parameter. σ gives the combined uncertainty on the medians.

clumpiness than expected from the trend displayed at longer wavelengths, they exhibit the same behavior of increasing clumpiness with decreasing wavelength. The systematically lower baseline difference can be explained by the relatively poor resolution of the *GALEX* data. The late-type spiral, irregular, and peculiar galaxies show the same trends in A and S , but a weaker relationship in C , where the concentration index changes little overall with observed wavelength.

Our previous study (Taylor-Mager et al. 2007) contained too few E/S0 galaxies in FUV and NUV to include significant data points on this plot. In that study, the optical/NIR data showed little to no indication of a dependence of CAS parameters on wavelength for E/S0 galaxies, but the *HST* near-mid-UV indicated a sudden, drastic decrease in C and a mild increase in A , when transitioning toward shorter wavelengths in the UV. However, the uncertainties on the *HST* data were relatively large, and they were based on few galaxies (2–4 per median data point). As such, we included the caveat that these rather surprising conclusions were only tentative.

The superior number statistics and smaller uncertainties of this *GALEX* study confirm an interesting transition in the morphologies of E/S0 galaxies when viewed in the mid- to far-UV. As seen in Figure 5, E/S0 galaxies are significantly less concentrated, more asymmetric, and slightly more clumpy than at redder colors, where the CAS parameters do not vary much with wavelength. Tests with the F300W data show that the clumpiness parameter for the inherently smooth E/S0 galaxies is not significantly affected by resolution, so we do not expect much of a correction for the low-resolution far-UV *GALEX* data. This dramatic change in A and the more mild change in S were not apparent from the Taylor-Mager et al. (2007) *HST* UV data.

Table 3 lists the differences in the median CAS parameters between the NUV and the FUV for each type bin (δ) and the errors on these differences (σ). This provides a quantitative correction between these structural parameters as measured at these two rest-frame wavelengths. These differential values show that there is a very significant drop in concentration for E/S0 galaxies when comparing the FUV to the NUV ($\delta_C(\text{E/S0}) = 0.45 \pm 0.11$). This is more extreme than the drop in C for early-mid-type spirals ($\delta_C(\text{Sa-Sc}) = 0.10 \pm 0.03$). Within the uncertainties, there is no change in C for late-type spirals, irregulars, and peculiars. All galaxy types are significantly more asymmetric in the FUV than the NUV, with the largest difference being for early- to mid-type spirals. Spiral, irregular, and peculiar galaxies are all significantly more clumpy in the FUV than the NUV, but E/S0 galaxies are only more clumpy by slightly more than 1σ .

4. Conclusions

In conclusion, we have measured the CAS parameters of 2073 nearby galaxies imaged in the far-UV by *GALEX*, and we release those values for use in future comparison studies, such as those with deep *HST* and *JWST* images.

We find a significant morphological k-correction in C for E/S0 and Sa-Sc galaxies, with decreasing concentration at shorter wavelengths. There is a particularly dramatic difference in concentration for E/S0 galaxies between the far- and mid-UV. Sd-Im and peculiar/merging galaxies show a weaker trend in C , where concentration does not vary much between filters. There is a strong morphological k-correction in A for all galaxy types, with increasing asymmetry at shorter wavelengths. However, there is little change in A for E/S0 galaxies within optical and IR wavelengths. There is also a strong k-correction in S of increasing clumpiness at shorter wavelengths for spirals, irregulars, and mergers/peculiars. For these galaxy types, we find that care should be taken when comparing images of vastly different spatial resolutions, as much lower resolution leads to a much lower clumpiness value. This resolution effect is not as strong for the inherently smooth E/S0, for which we find little dependence of S on wavelength, except for a mild increase in clumpiness when transitioning from optical to UV wavelengths. The A values, on the other hand, are not significantly affected by image resolution, which show that asymmetries are large-scale features that do not disappear at the lower (5 arcsec stellar FWHM) *GALEX* resolution.

The relationship between the CAS parameters and the observed rest-frame wavelength makes galaxies in general appear more late type than they really are at shorter wavelengths, especially in the mid- to far-UV, where the morphologies with CAS become nearly degenerate for all but the early-type galaxies (as is apparent in Figures 3 and 4). Surprisingly, this effect is so strong for E/S0 galaxies in the far-UV that their concentrations and asymmetries more closely resemble those of spirals and peculiar/merging galaxies at red optical wavelengths. These high asymmetries and low concentrations of ellipticals and lenticulars at shorter wavelengths can be explained by extended ultraviolet disks and halos that have been found in many spiral and irregular galaxies, where low-level star formation is ongoing in the faint outskirts (e.g., Holwerda et al. 2012; Hodges-Kluck et al. 2016). Most surprisingly, early-type (E/S0) galaxies historically considered to be “red and dead” have been found to be UV-bright (Schawinski et al. 2007), many with extended disks visible primarily in the UV (Rutkowski et al. 2012; Petty et al. 2013). This accounts for their diffuse and asymmetric structure as measured here in the UV, resulting in morphologies that more resemble those of disk galaxies in the optical. This UV excess in early-type galaxies can potentially be explained by recent star formation, or an evolved horizontal branch stellar population (O’Connell 1999; “UV upturn”). The stellar populations in the inner regions of some E/S0 galaxies have been found to be older than the outer regions (Petty et al. 2013), with more recent star formation in extended H I-rich regions (Yildiz et al. 2017). In at least some cases, this may be the result of recent interactions with companion galaxies or gas-rich merger events (George & Zingade 2015).

We thank the peer reviewer for the careful review of our paper. This research has made use of the NASA/IPAC Extragalactic Database (NED), which is operated by the Jet

Propulsion Laboratory, California Institute of Technology, under contract with the National Aeronautics and Space Administration. This research has also made use of NASA's Astrophysics Data System. The research was funded by NASA grant NNX09AF83G. R.A.W. is supported by NASA *JWST* Interdisciplinary Scientist grants NAG5-12460, NNX14AN10G, and 80NSSC18K0200 from GSFC.

Facilities: *GALEX*, *HST*.

ORCID iDs

Christopher J. Conselice  <https://orcid.org/0000-0003-1949-7638>

Mark Seibert  <https://orcid.org/0000-0002-1143-5515>

Barry F. Madore  <https://orcid.org/0000-0002-1576-1676>

Rogier A. Windhorst  <https://orcid.org/0000-0001-8156-6281>

References

- Bershady, M., Jangren, A., & Conselice, C. J. 2000, *AJ*, 119, 2645
- Bertin, E., & Armouts, S. 1996, *A&A*, 117, 393
- Bianchi, L. & GALEX Science Team 1999, *MmSAI*, 70, 365
- Bohlin, R. C., Cornett, R. H., Hill, J. K., et al. 1991, *ApJ*, 368, 12
- Conselice, C. J. 2003, *ApJS*, 147, 1
- Conselice, C. J. 2006, *MNRAS*, 373, 1389
- Conselice, C. J., Bershady, M. A., & Jangren, A. 2000, *ApJ*, 529, 886
- Conselice, C. J., Blackburne, J. A., & Papovich, C. 2005, *ApJ*, 620, 564
- Delgado-Serrano, R., Hammer, F., Yang, Y. B., et al. 2010, *A&A*, 509, 78
- Driver, S. P., Windhorst, R. A., Ostrander, E. J., et al. 1995, *ApJL*, 449, L23
- George, K., & Zingade, K. 2015, *A&A*, 583, A103
- Hodges-Kluck, E., Cafmeyer, J., & Bregman, J. N. 2016, *ApJ*, 833, 58
- Holwerda, B. W., Pirzkal, N., & Heiner, J. S. 2012, *MNRAS*, 427, 3159
- Kriek, M., van Dokkum, P. G., Franx, M., Illingworth, G. D., & Magee, D. K. 2009, *ApJ*, 705, 71
- Kuchinski, L. E., Freedman, W. L., Madore, B. F., et al. 2000, *ApJS*, 131, 441
- Kuchinski, L. E., Madore, B. F., Freedman, W. L., & Trewhella, M. 2001, *AJ*, 122, 729
- Mantha, K. B., McIntosh, D. H., Brennan, R., et al. 2018, *MNRAS*, 475, 1549
- Martin, C. & GALEX Science Team 2005, *IAUS*, 216, 221
- Martin, C. & GALEX Science Team 2009, *BAAS*, 41, 373
- Mortlock, A., Conselice, C. J., Hartley, W. G., et al. 2013, *MNRAS*, 433, 1185
- Nagashima, M., Yoshii, Y., Totani, T., & Gouda, N. 2002, *ApJ*, 578, 675
- O'Connell, R. W. 1999, *ARA&A*, 37, 603
- Petrosian, V. 1976, *ApJL*, 209, 1
- Petty, S. M., Neill, J. D., Jarrett, T. H., et al. 2013, *AJ*, 146, 77
- Rutkowski, M. J., Cohen, S. H., Kaviraj, S., et al. 2012, *ApJS*, 199, 4
- Schawinski, K., Kaviraj, S., Khochfar, S., et al. 2007, *ApJS*, 173, 512
- Seibert, M., Wyder, T., Neill, J., et al. 2012, *BAAS*, 219, 340.01
- Taylor-Mager, V. A., Conselice, C., Windhorst, R., & Jansen, R. 2007, *ApJ*, 659, 162
- Vika, M., Bamford, S. P., Haubler, B., et al. 2013, *MNRAS*, 435, 623
- Windhorst, R. A., Cohen, S. H., Hathi, N. P., et al. 2011, *ApJS*, 193, 27
- Windhorst, R. A., Hathi, N. P., Cohen, S. H., et al. 2008, *AdSpR*, 41, 1965
- Windhorst, R. A., Taylor, V. A., Jansen, R. A., et al. 2002, *ApJS*, 143, 113
- Yildiz, M. K., Serra, P., Peletier, R. F., Oosterloo, T. A., & Duc, P.-A. 2017, *MNRAS*, 464, 329